A&A 513, A10 (2010)
DOI: 10.1051/0004-6361/200913572

Astronomy & Astrophysics

An H I absorbing circumnuclear disk in Cygnus A

C. Struve[1,2] and J. E. Conway[3]

[1] Netherlands Foundation for Research in Astronomy, Postbus 2, 7990 AA Dwingeloo, The Netherlands
e-mail: struve@astron.nl
[2] Kapteyn Institute, University of Groningen, Landleven 12, 9747 AD Groningen, The Netherlands
[3] Onsala Space Observatory, 439 92 Onsala, Sweden
e-mail: john.conway@chalmers.se

Received 29 October 2009 / Accepted 19 December 2009

ABSTRACT

We present Very Long Baseline Array (VLBA) H I absorption observations of the core region of the powerful radio galaxy Cygnus A. These data show both broad ($FWHM$ = 231 ± 21 km s^{-1}) and narrow ($FWHM$ < 30 km s^{-1}) velocity width absorption components. The broad velocity absorption shows high opacity on the counter-jet, low opacity against the core and no absorption on the jet side. We argue that these results are most naturally explained by a circumnuclear H I absorbing disk orientated roughly perpendicular to the jet axis. We estimate that the H I absorbing gas lies at a radius of ∼80 pc has a scale height of about 20 pc, density $n > 10^4$ cm^{-3} and total column density in the range 10^{23}–10^{24} cm^{-2}. Models in which the H I absorption is primarily from an atomic or a molecular gas phase can both fit our data. Modelling taking into account the effective beam shows that the broad H I absorbing gas component does not cover the radio core in Cygnus A and therefore does not contribute to the gas column that blocks our view of the hidden quasar nucleus. If however Cygnus A were observed from a different direction, disk gas on ∼100 pc radius scales would contribute significantly to the nuclear column density, implying that in some radio galaxies gas on these scales may contribute to the obscuration of the central engine. We argue that the circumnuclear torus in Cygnus A contains too little mass to power the AGN over >10^7 yr but that material in the outer H I absorbing gas disk can provide a reservoir to fuel the AGN and replenish torus clouds. The second narrow H I absorption component is significantly redshifted (by 186 km s^{-1}) with respect to the systemic velocity and probably traces infalling gas which will ultimately fuel the source. This component could arise either within a tidal tail structure associated with a recent (minor) merger or be associated with an observed infalling giant molecular cloud.

Key words. galaxies: elliptical and lenticular, cD – galaxies: individual: Cygnus A – galaxies: kinematics and dynamics – galaxies: structure – galaxies: ISM – galaxies: active

1. Introduction

Circumnuclear obscuring tori/disks are an essential component of unified schemes of active galactic nuclei (e.g. Antonucci 1993; Tadhunter 2008). Recently there has been much progress in obtaining direct evidence for such structures especially in Seyfert luminosity objects. This evidence includes modelling of the IR SEDs from AGN heated dust in clumpy tori (Nenkova et al. 2008b) and direct IR interferometric imaging of this dust on 1–10 pc scales (Jaffe et al. 2004; Tristram et al. 2009).

On larger scales adaptive optics IR observations of molecular hydrogen lines (Hicks et al. 2009) have revealed geometrically thick gas at radii 30 pc in Seyferts. Additionally millimetre interferometry also detects molecular gas in emission on scales r = 70 pc (e.g. Schinnerer et al. 2000) albeit in more flattened disk-like structures. Such outer disk structures may be continuous with inner obscuring tori and provide both the fuel and a conduit for feeding the central engine. The relationship between these circumnuclear disks and obscuring tori is however far from clear.

Radio observations provide another means to study the circumnuclear gas environment. This can for instance be achieved by VLBI observations of maser emission from molecular gas (Lo 2005), free-free absorption from ionised gas and absorption from atomic gas (H I). Examples of the use of the latter two tracers include observations of NGC 1275 (e.g. Vermeulen et al. 1994), Centaurus A (e.g. Jones et al. 1996; Morganti et al. 2008), Hydra A (e.g. Taylor 1996), NGC 4261 (van Langevelde et al. 2000; Jones et al. 2001) and 1946 + 708 (Peck & Taylor 2001). Because of their high spatial resolution such radio observations are especially suitable for studying circumnuclear obscuring matter in powerful narrow line radio galaxies which are expected (see Tadhunter 2008) to be unified via orientation with radio-loud quasars. There is strong evidence from X-ray observations (Hardcastle et al. 2009) for the expected obscuration by large column densities in the former objects, however they are usually too distant and faint for optical and IR observations to directly observe the circumnuclear gas.

A prime target for studies of circumnuclear gas in a luminous "hidden quasar" radio galaxy is the closest Fanaroff-Riley (Fanaroff & Riley 1974) type II (FR-II) radio-galaxy Cygnus A. Spectropolarmetric observations of this source which revealed a hidden BLR in scattered light (Ogle et al. 1997) were a major milestone in the general acceptance of the orientation unification scheme for powerful radio galaxies and radio-loud quasars. Further evidence for shadowing from a central torus comes from the bi-cones observed in both optical emission lines (Jackson et al. 1998) and IR continuum (Tadhunter et al. 1999). The sharpness of the edges of these bi-cones suggest that the inner face of any torus occurs at radii <50 pc from the central engine (Tadhunter 2008). Tadhunter et al. (2003) have from optical/IR emission line observations measured a

rotation curve from gas rotating around the bi-cone/radio-jet axis at $r \approx 300-1000$ pc allowing a central black hole mass to be estimated. These observations may trace the outer parts of a circumnuclear gas structure which connects with the inner obscuring torus. The ultimate origin of this material could be related to the merger activity detected in Cygnus A (Canalizo et al. 2003).

The central radio core and inner jets of Cygnus A are relatively bright from millimetre to centimetre wavelengths allowing searches in absorption to constrain circumnuclear gas properties on small (<100 pc) scales. Molecular absorption observations so far give ambiguous results with only upper limits or marginal detections being reported (see e.g. Barvainis & Antonucci 1994; Fuente et al. 2000; Salomé & Combes 2003; Impellizzeri et al. 2006). VLBI observations by Krichbaum et al. (1998) have however found evidence for ionised circumnuclear gas on scales <20 pc via the detection of free-free absorption toward the counter-jet. Additionally Conway & Blanco (1995) detected broad H I absorption toward the core in VLA observation which were interpreted in terms of a circumnuclear disk/torus model, with the H I absorption either tracing the small atomic fraction of a mainly molecular medium or a purely atomic structure. To better constrain the scale and geometry of this H I absorbing gas we have performed high resolution NRAO Very Long Baseline Array (VLBA[1]) H I absorption observations. A short report on a initial reduction of this data was given by Conway (1999), this present paper presents a fuller re-analysis of the data. The organisation of this paper is as follows, in Sect. 2 we describe the observations while Sect. 3 presents the observational results including modelling of opacity profiles along the source. A discussion of the results is given in Sect. 4 and a summary in Sect. 5. At the redshift of Cygnus A ($z = 0.056$) for cosmologies with $H_0 = 73$ km s^{-1} 1 mas corresponds to approximately 1 pc, a scaling which we adopt throughout this paper. All total recession velocities quoted are heliocentric (optical definition).

2. Observations

Observations were performed on August 31st 1995 using the ten stations of the VLBA plus the phased VLA. Two IFs (left and right circular polarisation) with a bandwidth of 12.5 MHz and 256 channels were centred at the frequency of the previously observed H I absorption (~1340 MHz, Conway & Blanco 1995). A number of bright compact sources were observed as fringe finders and for bandpass calibration. The data were correlated in Socorro, USA. A standard data reduction using AIPS was performed including fringe fitting, calibration and flagging of the data. Cygnus A lies at a relatively low galactic latitude ($b = 5\overset{\circ}{.}7$) and the effects of interstellar scattering are significant at VLBI resolution. For this reason four antennas which participated only in long baselines, namely Brewster, Hancock, Mauna Kea and St. Croix showed no fringes to Cygnus A and so were deleted from the subsequent data analysis. Initial amplitude calibration was accomplished for VLBA antennas using the recorded system temperature values (which took into account the dominant contribution to the noise from the lobes of Cygnus A). For the phased VLA the calibrator $T_{\rm ant}/T_{\rm sys}$ values were used with a correction applied to take into account the system noise contribution from Cygnus A. Offsets in the VLA amplitude calibration scale were then corrected by comparing the correlated Cygnus A flux densities on long baselines to respectively the VLA and Pie Town. Initial continuum images were made via iterative phase self-calibration/deconvolution starting from a point source. A couple of cycles of amplitude and phase self-calibration were performed at the very end to obtain a noise limited continuum map.

Extensive experiments were carried out to determine the optimum uv weighting which gave the best combination of sensitivity and resolution for both continuum and spectral line. Final images were made using uniform weighting with robustness factor 0.5; giving rise to an almost circular dirty beam with main lobe width $FWHM \approx 25$ mas. Since the uv point weights also took into account the sensitivity of each baseline (by weighting by 1/noise variance) the final continuum and spectral line images are dominated by the baselines to the VLA. CLEAN images were restored with a circular $FWHM$ 25 mas Gaussian; however the effective image resolution is less than this because of the effects of foreground interstellar scattering. The observed effective resolution (i.e. the clean beam convolved with the interstellar scattering) is 32.7 mas, as determined by measuring the $FWHM$ of the continuum profile perpendicular to the jet at the core position – implying an interstellar scattering contribution of 21 mas.

The resulting continuum image (see Fig. 1) has rms noise of 0.43 mJy beam^{-1} and shows besides the unresolved core a jet and counter-jet structure (see Sect. 3). In principal it is possible that the counter-jet structure could be an artefact of phase self-calibration starting from a point source. To check this possibility we re-mapped the data only allowing flux density on the jet side to be included in the model in the initial cycles, but in all cases emission on the counter-jet side remained. The existence of a counter-jet is also confirmed by other observations (e.g. Krichbaum et al. 1998). In making our final continuum and spectral line images we used data self-calibrated against continuum models including both jet and counter-jet emission. Before making our spectral line cube we removed the continuum contribution using the AIPS task UVLIN and then imaged using the same weighting as used for our continuum image and the same CLEAN restoring beam. In order to increase sensitivity when creating our spectral line cube the uv data were averaged in frequency to give a final channel separation equivalent to 14.0 km s^{-1} in velocity or a velocity resolution of 28.0 km s^{-1} after Hanning smoothing. The noise achieved in the final line cube was $\sigma_{\rm rms} = 2.36$ mJy beam^{-1} per channel.

3. Results

3.1. Continuum image

The 1340 MHz continuum image (Fig. 1, top panel) is very similar to the 1660 MHz image shown by Krichbaum et al. (1998). We clearly detect the unresolved core, the jet and the weaker counter-jet (SE of the core). The PA of the jet is 105° ± 2°, in agreement with VLBI observations at higher frequencies (Krichbaum et al. 1998) and the kpc-size jet structure (Carilli et al. 1991). The continuum peak has brightness 0.16 Jy beam^{-1} and the total continuum flux recovered in our observations is 0.50 Jy.

3.2. HI absorption

An integrated absorption spectrum over our spectral line cube is shown in Fig. 1, bottom left. Broad ($\Delta v = 456$ km s^{-1}) H I absorption is detected in the velocity range from 16 679 to 17 135 km s^{-1} with the peak being located at $v = 17\,002$ km s^{-1} ($z = 0.05667$). The integrated spectrum is well fitted by two

[1] The VLBA is operated by the National Radio Astronomy Observatory which is a facility of the National Science Foundation operated under co-operative agreement by Associated Universities, Inc.

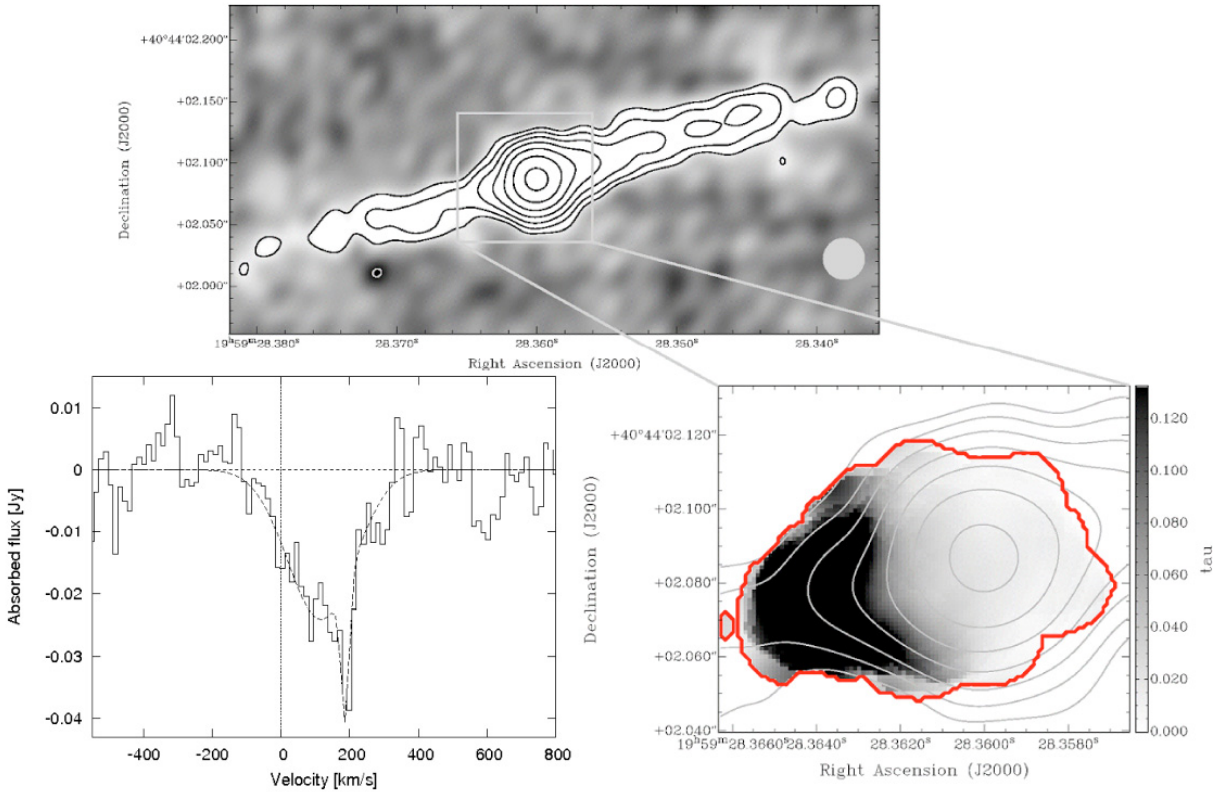

Fig. 1. *Top panel*: continuum image at 1340 MHz. The lowest contour is at 2 mJy beam^{-1} with subsequent contours increasing by factors of 2. The effective beam *FWHM* (see Sect. 2) is indicated in the lower right corner. *Bottom left panel*: integrated absorption spectrum from the blanked cube with the velocities shifted to the rest frame of Cygnus A (see Sect. 4.1). The dashed line shows the two component Gaussian fit. *Bottom right panel*: contours show continuum. Grayscale shows the mean opacity over the rest frame velocity range −80 to +170 km s^{-1}. The thick dark line shows the un-blanked region over which the integrated absorption spectra (shown in *the bottom left panel*) is calculated.

Gaussian components, yielding centroid velocities of 16 916 ± 10 km s^{-1} (z = 0.05639 ± 0.00003) and 16 986 ± 5 km s^{-1} (z = 0.05662 ± 0.00002), with *FWHM* = 231 ± 21 and 29 ± 10 km s^{-1} respectively (after correcting the line widths to the rest frame of the host galaxy). The second, narrow component has a *FWHM* velocity width similar to our velocity resolution and hence we consider this velocity width as an upper limit of the true line width. The presence of two components in the integrated spectrum suggests that the H I absorption consists of two different overlapping structures. Despite small differences in the flux scale (for continuum and absorption spectrum) the VLBA data agree in absorption width, profile shape and radial velocity with the VLA A- and B-array observations of Conway & Blanco (1995). These authors found slightly different Gaussian fits for the absorption spectrum, their data however potentially suffers from bandpass calibration and continuum subtraction problems (since two IFs – only slightly overlapping in velocity – had to be used to achieve sufficient spectral resolution and velocity coverage). Given these issues we conclude that both data sets agree within the noise of both observations so that we have recovered the full absorption seen by the VLA. The difference seen in flux scale between our VLBI and the published VLA observations are likely due to inaccuracies in amplitude calibrations of the VLA. This instrument, unlike VLBI, did not record the antenna system temperatures which are greatly enhanced due to the presence of the bright radio lobes of Cygnus A in the primary beam of each antenna, complicating the amplitude calibration.

Inspection of the data cube shows that the absorption is spatially resolved and is detectable over 95 mas in angle along the radio axis (i.e. ∼3 effective beam *FWHM*s). Below the second contour of the continuum image it is not possible to constrain the H I absorption because the background is too weak. The deepest absorption measured in mJy is toward the counter-jet and unresolved core but the highest opacities occur for the broad velocity component on the counter-jet side (see Fig. 1, bottom right). We find no indication of changes in spectral line absorption profiles in directions perpendicular to the jet axis – which is as expected given the small jet width (Krichbaum et al. 1998) compared to our effective resolution; this means we need to only consider the spectral profile as a function of position along the jet axis as shown in Fig. 2. In this figure the top panel shows the rotated continuum image while the middle panel shows the absorbed flux density (contours) and absorbed flux/continuum ratio (colours; note: saturated over 0.2) versus velocity and position along the jet.

The highest contours in the middle panel of Fig. 2 belong to the narrow velocity absorption component at recession velocity 16 986 km s^{-1} seen against the core. At the same velocity a slight extension on the jet-side is detectable, consistent with having the same $\tau \approx 0.1$ opacity as seen on the core. Because of the rapid fall-off of continuum intensity further along the jet and counter-jet further information about the spatial distribution of the narrow velocity component is limited. That is to say that the underlying continuum is not strong enough to detect the narrow velocity absorption component even if the opacity remains $\tau \approx 0.1$.

The broad absorption component in Fig. 2, middle panel (seen at velocities around 16 900 km s^{-1}) is detected from the core position out to 65 mas along the counter-jet. Over this

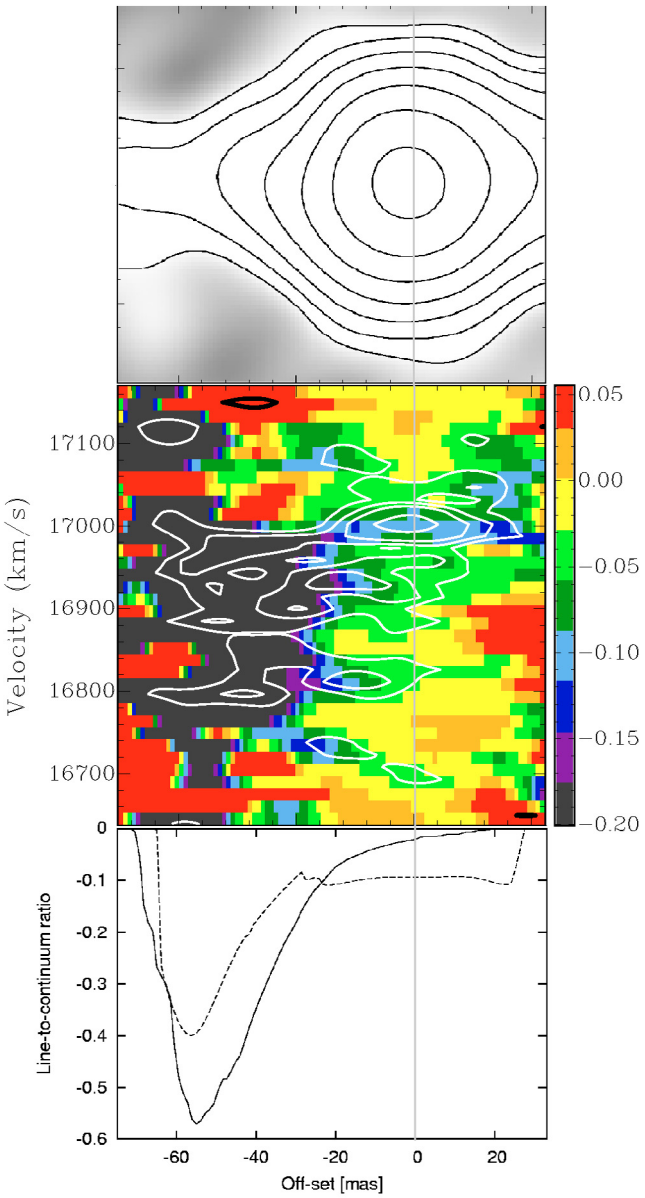

Fig. 2. *Top panel*: radio continuum image of the core region rotated such that the jet is pointing to the right and the counter-jet to *the left*. Contour levels are the same as in Fig. 1. *Middle panel*: position-velocity diagram along the radio axis. Grey scale shows the line-to-continuum ratio. Over-plotted in contours is the absorbed flux density in mJy beam^{-1}. Contour levels are −15, −10, −7.5, −5.0 (white) and 5.0 mJy beam^{-1} (black). *Bottom panel*: velocity averaged line-to-continuum ratio along the source for two different velocity ranges. The solid line is for a velocity range dominated by the broad velocity component (16 720−16 970 km s^{-1}), the dashed line for a velocity range (16 971−17 012 km s^{-1}) centred on the narrow absorption system velocity.

spatial range the broad component has absorbed flux densities (contour levels) which stay almost constant; given the rapid fall off in background continuum this corresponds to a rapid increase in line-to-continuum ratio (colours). Over the range of position from −50 mas to −65 mas spectra taken show the absorption to be flat bottomed and the absorbed flux density comparable with the continuum, both implying H I opacities $\tau \gg 1$. The absorption shows an apparent sharp decrease beyond −65 mas, though in a region with very weak continuum (we discuss further the reality of this decrease in Sect. 3.3). The broad absorption also apparently has a small but significant opacity ($\tau \approx 0.03$) at the position of the core, however, this may be due only to the limited spatial resolution causing "leakage" of absorption onto the core position. Quantitative estimates of broad line opacity along the source are made in Sect. 3.3 where the above two points are addressed.

Reinforcing the above description of the two velocity components the bottom panel of Fig. 2 shows the line to continuum ratio averaged over different velocity ranges versus position. The solid line shows average line-to-continuum for velocity ranges where the broad component dominates, while the dashed line is for a velocity range where the narrow absorption is most dominant. The broad component shows rapidly increasing absorption along the counter-jet reaching a peak velocity averaged line-to-continuum ratio of almost 0.6 at −55 mas (with peak ratios within the velocity profile at this position in fact reaching up to 1 and beyond). The second profile (dashed line) for the velocity range where the narrow velocity component normally dominates has approximately the same mean opacity on the core and jet. On the counter-jet side the average opacity over this velocity range increases, this is however consistent with the narrow absorption component having the same opacity as on the core and jet-side but with the average line-to-continuum ratio becoming dominated by contamination from the high velocity wings of the broad velocity component.

3.3. Modelling spatial variations in broad line opacity

The increase in line-to-continuum ratio of the broad absorption seen on the counter-jet side (see Sect. 3.2 and Fig. 2) implies a rapid increase in opacity. As noted in Sect. 3.2, at the position of maximum absorption the spectral profiles are flat-bottomed and saturated implying large opacity. To more accurately convert the line-to-continuum ratios versus velocity to peak opacity, and therefore estimate H I column density variations, we have carried out a detailed modelling of the data. In this modelling we describe both continuum and peak opacity estimates with a set of seven point sources separated by 15 mas along the jet/counter-jet axis (i.e. just under half an effective beam *FWHM* width). Additionally by taking into account the effective beam width this modelling provides a modest super-resolution of the data, important because interstellar scattering limits our spatial resolution (Sect. 2). Specifically, we are interested in the question of whether the weak broad absorption apparently seen at the core position (see Fig. 1 bottom right panel) is real or whether it can be explained by the combination of very strong absorption on the counter-jet side combined with limited spatial resolution.

In our modelling we first made estimates for the underlying continuum profile for each model point source (referred to as a "pixel") where there was detectable absorption. Continuum intensities were varied at each of these seven pixels until after convolution with the effective restoring beam the model continuum profile versus position fitted the observations. In a similar way we estimated for each pixel the absorbed line area (mJy km s^{-1}) at velocities in the range 16 720−16 970 km s^{-1} (where the broad absorption component dominates). Pixel values were again adjusted such that after convolution by the effective beam the model fitted the observations. Finally an estimate was made at each pixel of the peak H I opacity versus velocity by combining the pixel-based continuum and spectral line absorption estimates. In estimating this quantity we assumed the broad-component opacity spectrum was Gaussian with fixed velocity centroid and fixed *FWHM*.

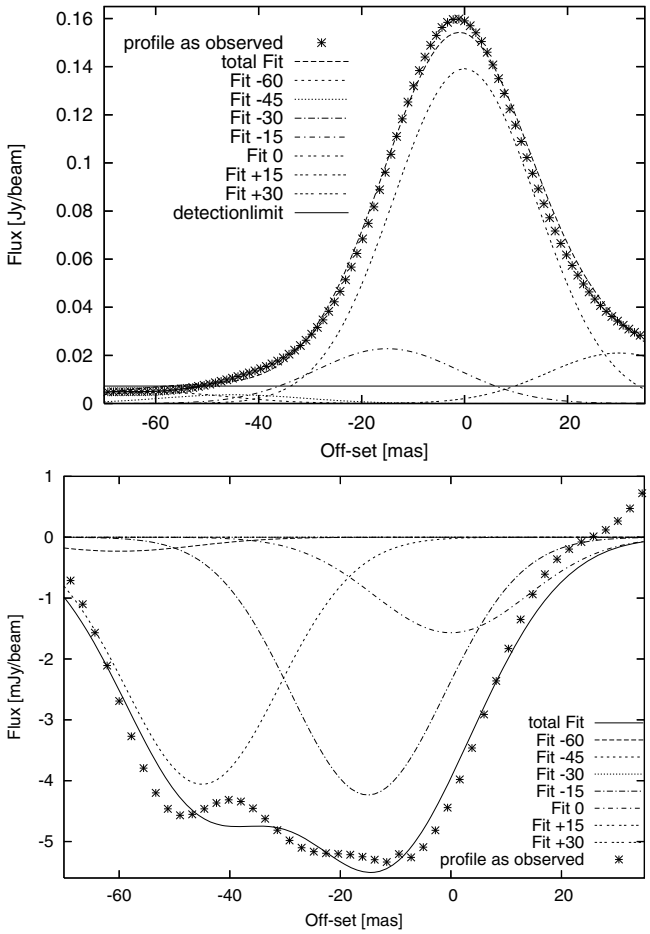

Fig. 3. Modelling of continuum and broad absorption along the jet axis (see Sect. 3.3). *Top panel*: comparison of model fit and data for the observed continuum profile found by adjusting pixel values while assuming an effective Gaussian beam of *FWHM* of 32.7 mas. *Bottom panel*: comparison of model and data for average absorbed line flux over the broad component velocity range from 16 720−16 970 km s^{-1}. In both plots negative offsets correspond to counter-jet, positive offsets to jet side.

The resulting fits reproduce (see Fig. 3), to first order, both the observed continuum and the absorbed flux profiles along the source. Deviations of the fits from the data are likely due to the background continuum being more complicated (see Krichbaum et al. 1998) than our parameterisation of it. Table 1 gives our results and the line centre peak opacity as plotted in Fig. 4. Note that no opacity estimate is plotted at positions −30 and +15 mas because the fitted continuum intensity at these positions was zero. We estimate the error of the line-to-continuum ratio (Table 1, Col. 4) assuming it is dominated by the rms noise in the line data. At position $r = -45$ mas the lower limit on line centre opacity is set by subtracting 2σ from the line-to-continuum ratio.

The peak opacity (Col. 5) takes into account that part of the absorption spectrum is flat bottomed and the attached error is calculated based on a $1\sigma_{\rm rms}$ uncertainty in our line data. Our results are consistent with no broad H I absorption on the jet-side and any opacity against the core being very low (0.016). Moving outward from the core along the counter-jet, the opacity increases and peaks at 45 mas ($N_{\rm H\,I} = 1.6 \times 10^{21}\ T_{\rm spin}$) before it sharply decreases to 0.078 at 60 mas from the core. Based on uncertainty estimates of the absorbed flux this drop in opacity is real and not an observational artefact due to insufficient signal-to-noise.

Table 1. Results of modelling of continuum and broad H I absorption profiles along the jet axis (see Sect. 3.3).

r (mas)	$F_{\rm C}$ (mJy)	$F_{\rm L}$ (mJy)	$F_{\rm L}F_{\rm C}^{-1}$	τ_0
–60	4.73	0.23	0.05 ± 0.12	0.080 ± 0.210
–45	3.62	4.06	1.12 ± 0.15	>3.110
–30	0.02	0.00	0.00	–
–15	22.78	4.24	0.19 ± 0.02	0.320 ± 0.040
0	139.16	1.57	0.01 ± 0.004	0.016 ± 0.006
15	0.00	0.00	–	–
30	20.98	0.00	0.00 ± 0.03	0 ± 0.0478

Notes. Column 1 give the distance from the core of the fitted pixel, negative offsets correspond to positions along the counter-jet, positive to positions on the jet side. Columns 2 to 4 give respectively the fitted continuum flux density, H I absorbed flux density averaged over fitted frequency range and the line to continuum ratio. Column 5 gives the modelled opacity at line centre.

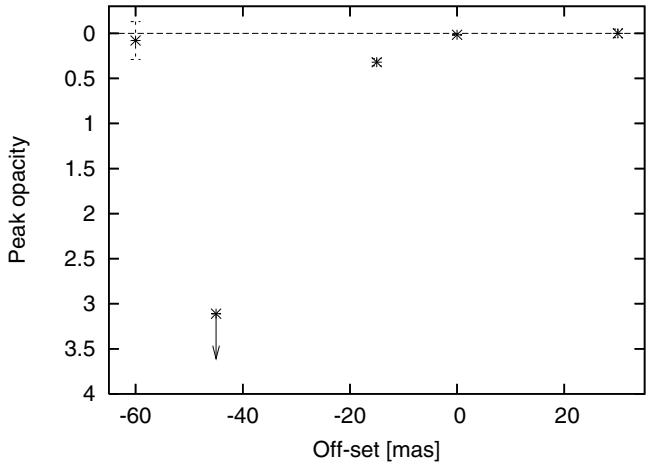

Fig. 4. Estimates of broad absorption opacity at line centre versus position along the radio axis after taking into account beam effects (see Sect. 3.3). The opacities and errors plotted are taken from Table 1.

4. Discussion

4.1. A disk geometry for the broad absorption component

The fact that the broad velocity width absorption is seen at high opacity only against the counter-jet and not against the jet is similar to the situation found for other powerful cores of radio galaxies observed in H I absorption, for instance in the FR-I source NGC 4261 (van Langevelde et al. 2000). The most natural explanation for these observations is that the H I absorption lies in a flattened structure roughly in a plane perpendicular to the radio axis (i.e. a circumnuclear disk). Alternative explanations involving foreground clouds in the ISM of the host galaxy seem unlikely, requiring within elliptical hosts a large covering factor of 10−100 pc sized clouds with uncharacteristically large internal velocity dispersion (of order 300 km s^{-1}).

Converting our observations of the location and distribution of H I absorption along the counter-jet to an exact of radius in the disk depends on the precise orientation of the disk. Over the range of plausible disk orientations however this radius varies over a fairly narrow range as can be seen by examining two

limits, first when the disk is close to edge-on and when at its maximum plausible tilt. In the former case the H I profile width in Fig. 4 measures the scale height of the disk. Since we know the central black hole mass ($M_{\rm BH} = 2.5 \times 10^9\ M_\odot$, Tadhunter et al. 2003) the radius at which the H I absorption occurs can be calculated (following Krolik & Begelman 1988) via:

$$\frac{\Delta h}{r} \sim \frac{\Delta v}{v_{\rm rot}(r)} \quad (1)$$

where Δh is the disk scale height, r the radius from the core, $\Delta v = 98.5$ km s^{-1} the velocity dispersion (estimated from the Gaussian fit in Sect. 3.3) and $v_{\rm rot}(r)$ the Keplerian rotation velocity at radius r from the central black hole. Assuming $\Delta h = 25$ pc and solving for r we obtain $r = 88$ pc. In the other limit we consider a maximally inclined disk. Based on VLBI observations of the jet to counter-jet brightness ratio of the parsec scale jet (Krichbaum et al. 1998) the jet axis is orientated at an angle $\theta > 80°$ to the line of sight. Based on measured misalignments of larger scales (Tadhunter et al. 2003) we estimate a maximum misalignment between disk and radio axes of 30° – which gives a maximally inclined disk which is 40° from edge-on. The peak H I opacity is observed to occur at projected distance 45 pc along the counter-jet which when de-projected corresponds to a radius of 70 pc. Using again Eq. (1) this gives a scale height of ∼18 pc. Based on the above two limits we will assume in the following that the H I peaks at a radius 80 pc from the black hole and has a scale height of about 20 pc. The resulting opening angle of the circumnuclear H I disk is ∼14° which is similar to what is found in other sources (e.g. in NGC 4261 van Langevelde et al. 2000).

An important question in considering the feasibility of the disk hypothesis is the velocity of the broad absorption relative to the systemic velocity of the galactic nucleus. For a disk which is perfectly normal to the jet axis these velocities will be the same. Our best estimate of the systemic velocity we take to be $z = 0.05600 \pm 0.00008$ (=16 800 ± 24 km s^{-1}) which is the mean of six published optical/IR emission line estimates (see Table 1 in Tadhunter et al. 2003). The centroid of the broad component at 16 916 km s^{-1} is therefore 116 km s^{-1} beyond the mean systemic velocity. The observed offset however can be accommodated if there were a fairly modest misalignment between the disk axis and the jet. VLBI observations constrain the jet axis to be within 10° of the sky plane. For such an orientation misalignments between projected jet axis and disk axis will be similar to intrinsic misalignments. Given the arguments above that the H I absorption occurs at ∼80 pc radius and given the estimated central black hole mass of ($M_{\rm BH} = 2.5 \times 10^9\ M_\odot$, Tadhunter et al. 2003) the orbital velocity is $v_{\rm rot}(r = 80\ {\rm pc}) = 367$ km s^{-1}. Given this orbital velocity a misalignment of only 21° is sufficient to explain the difference between the H I centroid and systemic velocities.

4.2. Physical properties of the broad absorption component gas

According to Maloney et al. (1996) the physical state of gas around an AGN is controlled by an ionisation parameter determined from the ratio of the hard X-ray photon flux to local gas density. At a given radius r this ionisation parameter equals

$$\xi_{\rm eff} = L_{\rm X} \cdot n^{-1} \cdot r^{-2} \cdot N_{22}^{-0.9} \quad (2)$$

where $L_{\rm X}$ is the luminosity in > 2 keV X-rays and n is the gas number density. The final term takes account of the effects of X-ray photoelectric absorption where N_{22} is the the column density in units of 10^{22} cm^{-2} (In Cygnus A X-ray observations give an estimate of $N_{22} = 20$ along the line of sight to the core, Young et al. 2002). According to the model of Maloney et al. (1996, see their Fig. 3) for Cygnus A at $r = 80$ pc the gas fraction is predominantly atomic (>90%) for a density range $10^3 < n < 1.6 \times 10^5$ cm^{-3}. The remaining <10% of the gas is ionised at low densities ($n = 10^3$ cm^{-3}) and becomes molecular at higher densities ($n \approx 10^5$ cm^{-3}). Above densities of 3.3×10^5 cm^{-3} the gas is mostly molecular.

The Maloney et al. (1996) model can be used to predict the disk H I and free-free absorption opacity as a function of gas density; comparison with observations can then constrain the density. In order to predict opacities we need to convert gas volume densities to column densities which requires estimates of the path length through the absorbing gas. Based on our estimate of the disk thickness of 20 pc and the maximum disk inclination angle with respect to the line of sight (Sect. 4.1) we estimate the geometric path length through the disk to be at least 31 pc. This is a strict lower limit and we adopt $L_{\rm geom} = 40$ pc as a more likely value. Note that if the gas exists in clouds the effective path length through absorbing gas can be less than $L_{\rm geom}$ but it cannot be larger. Using the above assumptions we find that upper limits on free-free absorption toward the counter-jet do not give any useful gas density constraints. This is because, although the free-electron fraction increases at lower densities this is compensated for by a lower total gas column such that the free-free opacity continuum absorption at 21 cm wavelength against the counter-jet is less than 0.1 over all reasonable densities.

For modelling H I absorption the relevant parameters given by Maloney et al. (1996) are the predicted gas temperature and atomic fraction versus effective ionisation parameter $\xi_{\rm eff}$. At the radius of the absorbing H I assuming densities high enough to give a predominately atomic (and not ionised) column, the increase of $T_{\rm spin}$ due to radiative excitation from the radio core is negligible (see e.g. Bahcall & Ekers 1969). Given this we assume the atomic gas is thermalised and that its spin temperature ($T_{\rm spin}$) equals the gas temperature (T). The predicted H I line width in this cases is proportional to $N_{\rm HI}T^{-1}$ where $N_{\rm HI}$ is the H I column density and T the temperature. Both of the above quantities can be calculated as functions of the local density n. The former quantity equals the product of the total column density $N = n \cdot L_{\rm geom}$ (for a uniform filled column) multiplied by the H I abundance. This abundance is a function of $\xi_{\rm eff}$ (calculated using Fig. 3 in Maloney et al. 1996) which in turn is a function of n via Eq. (2) (where $N_{22} = N/10^{22}$). Likewise T can be derived as a function of n, again using Fig. 3 in (Maloney et al. 1996). Combining the $N_{\rm HI}$ and T dependencies on n together we can predict $N_{\rm HI}T^{-1}$ and hence the expected H I absorption linewidth versus local density and then compare to observations. For densities $n > 10^4$ cm^{-3} the predicted H I absorption is larger than observed, this can however easily be reconciled with observations if the H I absorption is concentrated in clouds (see below). At densities $n < 10^4$ cm^{-3} however there are no solutions that can provide enough H I absorption to match what we observe, hence we can set a minimum density of 10^4 cm^{-3} for our H I absorbing gas.

For the gas density range 1.0×10^4 cm^{-3} $< n < 3.2 \times 10^4$ cm^{-3} there exist pure atomic phase gas solutions which fit the H I observations. These solutions require the absorption to occur in clouds such that only a fraction $f_{\rm LOS}$ of a typical LOS passes through clouds. At the higher densities within this range the requirements on total gas column density are reduced because gas/spin temperatures decline making hydrogen atoms more efficient at absorption. At the boundary in density between having predominately atomic or molecular phase clouds (at

density 4.6×10^4 cm^{-3}) the spin temperature is ~114 K the cloud line of sight filling factor is $f_{\rm LOS} = 0.032$ and $N = 1.82 \times 10^{23}$ cm^{-2} which is comparable to the X-ray absorption column along the line of sight to the central engine. At higher densities the clouds become predominately molecular but the observed H I absorption can still be fitted by similar total gas column densities. The reason is that although the atomic fraction declines rapidly with increasing density the temperature also declines, this increases the efficiency of absorption per hydrogen atom which almost exactly compensates for the reduced abundance.

In summary we cannot on the basis of our H I observations alone distinguish between models for the H I absorbing gas phase which are primarily atomic or molecular. We can however set at minimum density ($n > 10^4$ cm^{-3}) and a range for the total gas column density through the H I absorbing disk (10^{23} cm^{-2} $< N < 10^{24}$ cm^{-2}). Estimating total gas masses is complicated for those solutions invoking clouds in that these solutions only fix the line of sight filling factor, converting to volume filling factors requires knowing the cloud size, on which we have no constraint. For the minimum density solution where the gas column is continuous we can make a rough estimate of disk gas mass of $M_{\rm gas\ disk} = 1.0 \times 10^8\ M_\odot$ within the inner 80 pc radius of the disk. For higher density solutions, both total required column densities and cloud filling factors decrease so that total gas mass requirements are significantly less. In all cases the total disk mass is much less than that of the central black hole ($M_{\rm BH} = 2.5 \times 10^9\ M_\odot$, Tadhunter et al. 2003) which therefore dominates the kinematics in the inner part of the nucleus that we observe.

4.3. Constraints on circumnuclear torus properties and relation to the H I disk

It is interesting that the estimated total gas column density through the H I absorbing gas (see Sect. 4.2) is comparable to that estimated by X-ray photoelectric absorption toward the core of 2×10^{23} cm^{-2} (see Young et al. 2002). Is it possible that most of this column density and most of the material that hides the quasar nucleus occurs as far out as $r = 80$ pc? An obvious problem with such a scenario is the absence of broad H I absorption along the direct line of sight to the radio core (peak opacity is $\tau_0 = 0.016 \pm 0.006$, compared to >1 on the counter-jet, see Sect. 3.3 and Fig. 2). A change in gas physical state with scale-height in the disk while keeping almost constant column density seems unlikely. If the high scale-height gas covering the core were still predominately atomic or molecular we find no density solutions that fit the low limit on H I absorption seen. On the other hand if the high scale height gas were wholly ionised at this column density it would strongly free-free absorb the radio core. Although there are signs of free-free absorption at $r \leq 20$ pc (Krichbaum et al. 1998) along the counter-jet this absorption does not cover the core position itself.

It seems likely instead that most of the X-rays absorbing column in Cygnus A and other hidden quasars occurs on scales $\ll$100 pc in a compact circumnuclear *torus*. The inner radius of such a torus is set by the dust sublimation radius, $r_{\rm d} = 0.4 \cdot (L_{\rm bol} \times 10^{-45}\ {\rm erg^{-1}\ s})^{0.5}$ pc (Nenkova et al. 2008b) where $L_{\rm bol}$ is the AGN bolometric luminosity. For Cygnus A $L_{\rm bol}$ is estimated to be 1.5×10^{45} erg s^{-1} (Whysong & Antonucci 2004) giving $r_{\rm d} = 0.5$ pc. It should be noted that the Whysong & Antonucci (2004) mid-IR estimate of the bolometric luminosity is significantly lower (by factors 5–20) than estimates based on the unabsorbed hard X-ray luminosity (see Tadhunter et al. 2003), possibly because of uncorrected torus extinction at mid-IR wavelengths (Tadhunter, private communication). However, an increase by a factor of 20 in bolometric luminosity results in the sublimation radius increasing only to $r_{\rm d} = 2.2$ pc, still significantly smaller than the radius of the H I structure. The outer radius ($r_{\rm out}$) is probably not as cleanly defined as in some early depictions of doughnut-like tori (Padovani & Urry 1992) and may even be continuous with larger circumnuclear disks (see references in Sect. 1). Consistent with these more general geometries the term "torus" can be thought of, if one prefers, as an acronym for "Thick/toroidal Obscuration Required by Unified Schemes" (Conway 1999; Elitzur 2008) rather than referring to a specific fixed geometry.

Recently Privon (2009) has fitted the observed Spectral Energy Distribution (SED) of the Cygnus A nucleus with a combined synchrotron jet, starburst and torus model. The torus fitting assumed the clumpy model of Nenkova et al. (2008a,b). A wide range of solutions were obtained depending on assumptions about the disk inclination and synchrotron jet spectrum. Most plausible solutions however had cloud number density per unit volume declining as r^{-q} with $q = 1$ and ratios of outer to inner radius, $Y = 30$ (giving $r_{\rm out} = 18$ pc for Cygnus A). Satisfyingly, the predicted total column density matches the X-ray absorption estimate within the errors. Despite the relatively large formal outer radius the concentration of clumps toward the inner edge means that most of the column density is concentrated at small radii. For a radial exponent of $q = 1$ half of the total column density occurs within $\sqrt{Y} \cdot r_{\rm in}$ corresponding to 2.8 pc, i.e. on a much smaller scale than our observed H I absorption.

The above results beg the question of relationship between the H I absorbing disk and the circumnuclear torus in Cygnus A. The mass in the torus is very low ($6 \times 10^5\ M_\odot$, following Elitzur 2008) and the lifetime of large scale-height clouds within it is short (due to intercloud collisions, see e.g. Krolik & Lepp 1989). Hence, both to fuel the quasar-like nucleus at the expected rate of $\sim 1\ M_\odot$ yr^{-1} and to replenish the torus clouds a much larger reservoir of material is required, which could reside in the H I absorbing disk. The mass in such a disk (see Sect. 4.2) is sufficient to power the source for 10^7 to 10^8 yr and may form part of a "feeding structure" which funnels gas from kilo-parsec scales into the central black hole. A feeding connection between disk and torus seems likely but the mechanisms of gas transport between the two scales is unclear.

Pertinent to the feeding question is whether the torus and the H I absorbing disk are a continuous structure with one gradually melding into the other, or if they are dynamically distinct and contain gas with very different physical conditions. The former possibility is motivated by the fitted torus outer radius $r_{\rm out} = 18$ pc which is of the same order of magnitude as the radius of the H I absorption ($r = 80$ pc). Furthermore the torus outer radius determined from SED fitting is not well constrained by the data and may extend beyond this limit. However, in such a continuous model for clouds with approximately fixed density the clouds would likely be in an increasingly molecular state over a projected radius from 1 to 70 pc as the excitation parameter decreased. It is hard to see how the rapid gradient in H I absorption seen along the counter-jet could be reproduced in such a case. Furthermore the observation of free-free absorption at intermediate positions ($r < 20$ pc, Krichbaum et al. 1998) is inconsistent with such a continuous model. It seems more likely that the torus – although ultimately fed from gas in the disk – is a distinct structure, perhaps generated in an accretion disk wind as in the model of Elitzur & Shlosman (2006). Clearly, more work is required to understand how the observed components in Cygnus A and other radio galaxies of 100 pc scale

H I absorbing disks, inner ionised gas and circumnuclear tori are connected in self-consistent structures which both obscure and feed the central engine.

An additional remark concerning the disk/torus interrelationship is that although in Cygnus A the H I absorbing disk likely does not contribute to the total absorbing column toward the central engine (as estimated from the X-ray observations) it could have done so if we had observed Cygnus A from a different direction.

Further progress on understanding the circumnuclear gas environment in Cygnus A probably requires the reliable detection of molecular absorption and its imaging with VLBI. Single dish searches at commonly observed molecular transitions such as the ground and higher rotational transitions of CO (Barvainis & Antonucci 1994; Salomé & Combes 2003) have so far yielded only upper limits. In contrast a tentative detection of CO+ in absorption using the IRAM 30 m was reported by Fuente et al. (2000) with a centroid velocity and *FWHM* velocity width (170 km s^{-1}) very similar to that of our broad H I absorption. This detection has yet to be confirmed interferometrically (Fuente, private communication). Given the results in this paper, despite the similarity in spectral shape, it seems unlikely that these observations are probing the same gas column as seen in H I absorption. The counter-jet which provides the background continuum against which the atomic hydrogen absorption is seen will have negligible flux density at millimetre wavelengths. Instead the line of sight probed at 3 mm wavelength will probably lie at projected distances <1 pc from the central engine. While this is comparable to the scales on which the circumnuclear torus has its largest column density (~3 pc) we would expect that the velocity dispersion of clouds in such a geometrically thick torus would be comparable to the orbital velocity at this radius (i.e. 1900 km s^{-1}), which is much broader than is observed. Similar considerations apply to the tentative VLBA observations of exited OH absorption reported by Impellizzeri et al. (2006) at projected radii <3 pc which only have observed width ~100 km s^{-1}.

4.4. The narrow absorption component

While we argue that the broad absorption component is caused by gas rotating around the central black hole (Sect. 4.1) the narrow (<30 km s^{-1} see Sect. 3) absorption gas is likely to have a different origin. This narrow velocity component is significantly redshifted (~186 km s^{-1}) with respect to the optical systemic velocity implying foreground gas moving inward toward the nucleus. This component is detected over the whole continuum region (i.e. jet, core and counterjet) where the observations are sensitive enough to detect an opacity of ~0.1 (see Sect. 3.2 and Fig. 2). A very similar opacity and centroid velocity is seen at the core position and one effective beam away on the jet side. The apparent increase in opacity at the velocity of the narrow absorption that is seen on the counter-jet side in Fig. 2 can be explained entirely by contamination by the broad velocity wings of the broad velocity absorption. While we do not have many independent samples of the narrow velocity component opacity versus position those we do have are consistent with a constant narrow component opacity of 0.1 over the whole VLBI radio source. Although the foreground distance from the narrow H I absorption to the VLBI continuum source is not well constrained we suspect that it must be >100 pc given its narrow velocity width and the position stability of its velocity centroid; if the gas was closer one would expect tidal forces to widen the velocity width and increase velocity centroid variations.

The structure and origin of the narrow H I absorption is unclear. Physically it could be related to a minor merging event, detected 400 pc South-West of the core (Canalizo et al. 2003). As a result of this interaction the narrow H I component could arise in a tidal tail of gas that is moving towards the nucleus. According to galaxy merger simulations (Bournaud et al. 2005) part of the progenitor's gas that gets expelled in tidal tails during a merging event will eventually fall back on the disk. The narrow component could also be connected to the giant infalling molecular cloud located 1.35 kpc to the North-West of the nucleus (Bellamy & Tadhunter 2004). However, the projected distances from the core are rather different such that a direct connection is not obvious. Both of the above gas components are relatively large (>100 pc) and thus would be consistent with having fairly constant H I opacity over the whole VLBI structure.

Further progress with constraining the size and origin of the narrow H I absorption system might be made by making future sensitive (and high spectral resolution) e-MERLIN or EVLA observations to try to trace the narrow H I absorption further along the jet.

5. Summary

We have presented VLBA H I absorption data of the core region of Cygnus A. H I absorption is detected over a linear scale of 95 pc, but is seen mainly along the counter-jet and on the nucleus. The integrated spectrum can be well-fitted by two Gaussian profiles suggesting a broad (*FWHM* = 231 ± 21 km s^{-1}) and a narrow (<30 km s^{-1}) component. Modelling the data shows that the broad absorption occurs only against the counter-jet and not against the jet. Against the unresolved core the opacity is very low. The broad velocity component can be explained by a circumnuclear disk which has its highest opacity 45 mas away (in projection) from the black hole. The narrow velocity component could be explained as an infalling tidal tail, presumably left from a past minor merging event.

The radius at which the broad H I absorption occurs can be constrained with the help of limits on the orientation of the disk. We find a relatively narrow range of possible parameters, resulting in an estimated radius of ~80 pc for the peak opacity, a disk scale height of about 20 pc and hence an opening angle of 14°. The offset between the centroid of the broad velocity component and the mean systemic velocity can be explained by a tilt of 21° of the disk axis compared to the jet axis.

Based on the derived geometry of the circumnuclear disk we derived physical properties of the H I absorbing gas. We find the minimum gas density to be $n > 10^4$ cm^{-3} with a spin temperature $T_{\rm spin} < 740$ K. With the H I observations alone we cannot distinguish between models for the H I absorbing gas phase which are primarily atomic or molecular. We can however set a range for the total gas column density through the H I absorbing disk of 10^{23} cm$^{-2} < N < 10^{24}$ cm^{-2}. An upper limit on the gas mass within a radius of 80 pc is $M_{\rm gas-disk} = 10^8\ M_\odot$, which is a factor 25 less than the black hole mass estimated by Tadhunter et al. (2003).

The circumnuclear torus in Cygnus A has an estimated fiducial radius ~ 3 pc, which is a much smaller scale than our observed H I absorption. The estimated mass in the torus clouds ($6{\cdot}10^5\ M_\odot$) is too low to power (alone) the source for 10^7–10^8 yr. In contrast the H I disk has enough mass to feed the AGN and replenish the torus clouds.

Higher sensitivity, broader band observations are needed to study the properties of the atomic circumnuclear disk in more detail, to search for a connection with the torus

and to investigate whether the torus contains a very broad (2000 km s^{-1} wide) H I absorption component. Higher spectral resolution e-MERLIN or EVLA observations of the narrow absorption component are needed to try to trace absorption further out along the jet to constrain its physical size.

Acknowledgements. This research was supported by the EU Framework 6 Marie Curie Early Stage Training programme under contract number MEST-CT-2005-19669 ESTRELA. J.C. acknowledges financial support from the Swedish Science Research Council. We thank the referee Clive Tadhunter for his comments that helped to improve the paper. We wish to thank Joan Wrobel of NRAO for extensive help in setting up the phased VLA for VLBI observations at a non-standard observing frequency.

References

Antonucci, R. 1993, ARA&A, 31, 473
Bahcall, J. N., & Ekers, R. D. 1969, ApJ, 157, 1055
Barvainis, R., & Antonucci, R. 1994, AJ, 107, 1291
Bellamy, M. J., & Tadhunter, C. N. 2004, MNRAS, 353, 105
Bournaud, F., Jog, C. J., & Combes, F. 2005, A&A, 437, 69
Canalizo, G., Max, C., Whysong, D., Antonucci, R., & Dahm, S. E. 2003, ApJ, 597, 823
Carilli, C. L., Perley, R. A., Dreher, J. W., & Leahy, J. P. 1991, ApJ, 383, 554
Conway, J. E. 1999, in Highly Redshifted Radio Lines, ed. C. L. Carilli, S. J. E. Radford, K. M. Menten, & G. I. Langston, ASP Conf. Ser., 156, 259
Conway, J. E., & Blanco, P. R. 1995, ApJ, 449, L131
Elitzur, M. 2008, New Astron. Rev., 52, 274
Elitzur, M., & Shlosman, I. 2006, ApJ, 648, L101
Fanaroff, B. L., & Riley, J. M. 1974, MNRAS, 167, 31P
Fuente, A., Black, J. H., Martín-Pintado, J., et al. 2000, ApJ, 545, L113
Hardcastle, M. J., Evans, D. A., & Croston, J. H. 2009, MNRAS, 396, 1929
Hicks, E. K. S., Davies, R. I., Malkan, M. A., et al. 2009, ApJ, 696, 448
Impellizzeri, V., Roy, A. L., & Henkel, C. 2006, in Proceedings of the 8th European VLBI Network Symposium
Jackson, N., Tadhunter, C., & Sparks, W. B. 1998, MNRAS, 301, 131
Jaffe, W., Meisenheimer, K., Röttgering, H. J. A., et al. 2004, Nature, 429, 47
Jones, D. L., Tingay, S. J., Murphy, D. W., et al. 1996, ApJ, 466, L63
Jones, D. L., Wehrle, A. E., Piner, B. G., & Meier, D. L. 2001, ApJ, 553, 968
Krichbaum, T. P., Alef, W., Witzel, A., et al. 1998, A&A, 329, 873
Krolik, J. H., & Begelman, M. C. 1988, ApJ, 329, 702
Krolik, J. H., & Lepp, S. 1989, ApJ, 347, 179
Lo, K. Y. 2005, ARA&A, 43, 625
Maloney, P. R., Hollenbach, D. J., & Tielens, A. G. G. M. 1996, ApJ, 466, 561
Morganti, R., Oosterloo, T., Struve, C., & Saripalli, L. 2008, A&A, 485, L5
Nenkova, M., Sirocky, M. M., Ivezić, Ž., & Elitzur, M. 2008a, ApJ, 685, 147
Nenkova, M., Sirocky, M. M., Nikutta, R., Ivezić, Ž., & Elitzur, M. 2008b, ApJ, 685, 160
Ogle, P. M., Cohen, M. H., Miller, J. S., et al. 1997, ApJ, 482, L37
Padovani, P., & Urry, C. M. 1992, ApJ, 387, 449
Peck, A. B., & Taylor, G. B. 2001, ApJ, 554, L147
Privon, G. C. 2009, [arXiv:0908.3476]
Salomé, P., & Combes, F. 2003, A&A, 412, 657
Schinnerer, E., Eckart, A., Tacconi, L. J., Genzel, R., & Downes, D. 2000, ApJ, 533, 850
Tadhunter, C. 2008, New Astron. Rev., 52, 227
Tadhunter, C. N., Packham, C., Axon, D. J., et al. 1999, ApJ, 512, L91
Tadhunter, C., Marconi, A., Axon, D., et al. 2003, MNRAS, 342, 861
Taylor, G. B. 1996, ApJ, 470, 394
Tristram, K. R. W., Raban, D., Meisenheimer, K., et al. 2009, A&A, 502, 67
van Langevelde, H. J., Pihlström, Y. M., Conway, J. E., Jaffe, W., & Schilizzi, R. T. 2000, A&A, 354, L45
Vermeulen, R. C., Readhead, A. C. S., & Backer, D. C. 1994, ApJ, 430, L41
Whysong, D., & Antonucci, R. 2004, ApJ, 602, 116
Young, A. J., Wilson, A. S., Terashima, Y., Arnaud, K. A., & Smith, D. A. 2002, ApJ, 564, 176